

# Probing the structural, elastic, electronic and thermoelectric properties of C15-type Laves phase $\text{LaCo}_2$ : a DFT based ab-initio investigation

S. Ziri<sup>a</sup>, L. Blaha<sup>a</sup>, F. Boukabrine<sup>b</sup>, A. Maafa<sup>a</sup>, A. Oughilas<sup>a</sup>, A. Bouabça<sup>a</sup> and H. Rozale<sup>a\*</sup>

<sup>a</sup>Condensed Matter and sustainable development Laboratory (LMCDD),  
University of Sidi Bel-Abbes, Sidi Bel-Abbes 22000, Algeria.

\*e-mail: hrozale@yahoo.fr; hrozale@univ-sba.dz

<sup>b</sup>The Study of Materials and Optical Instrumentation Laboratory (LEMIO),  
University of Sidi Bel-Abbes, Sidi Bel-Abbes 22000, Algeria.

Received 24 January 2021; accepted 8 March 2021

Using first-principles calculations based on density functional theory, structural, elastic, electronic and thermoelectric properties of Laves phase  $\text{LaCo}_2$  intermetallic compound with prototype  $\text{MgCu}_2$  are stated in this paper. The optimized lattice constant by structural optimization is found to be rationally compatible with the experimental lattice constant. The Generalized Gradient Approximation (GGA)+Hubbard model was incorporated to evaluate the exact electronic structure. Elastic properties such as elastic constants, bulk modulus  $B$ , shear modulus  $G$ , Young's modulus  $E$ , and Poisson ratio  $\nu$  have been determined using the Voigt-Reuss-Hill approximation. The ductility nature appears in both values of Cauchy pressure and Pugh's ratio. The band structures and the Cauchy pressure show that the material behaves as metallic. In addition, semi-classical Boltzmann theory is used to verify the applicability of the material for thermoelectric applications. Calculations depict that the spin-up/down transport coefficients are temperature-dependent. It has been found that  $\text{LaCo}_2$  has a high Seebeck coefficient and therefore a large power factor.

**Keywords:**  $\text{LaCo}_2$  intermetallic; FP-LAPW; mechanical stability; thermoelectric materials; laves phase.

**PACS:** 71.20.Lp; 78.20.Ci; 51.35.+a; 74.25.Fy; 61.50.Lt

**DOI:** <https://doi.org/10.31349/RevMexFis.67.041003>

## 1. Introduction

In recent years, Laves phase materials have been found to have unique properties, making them attractive for structural applications with high temperatures [1] and also to their usefulness in technical applications. Intermetallic compounds, which have been attractive for their Curie temperatures and the simple cubic laves-phase (C15) crystal structure, have also gained a great deal of attention from researchers due to the fascinating features of polymorphism, unusual magnetic properties, electrical properties and possible applications such as superconducting, giant magnetostrictive materials and hydrogen storage materials [2]. Cubic Laves phase intermetallic compounds  $\text{REX}_2$  (where RE= rare earth elements and X= transition metal) attracted a lot of attention due to peculiar meta-magnetic transitions that derive from the co-existence and interaction of magnetic moments of strongly localized RE 4f electrons and itinerant 3d electrons of the X [3]. Binary Laves phases with AB<sub>2</sub> composition are part of the topologically close-packed (TCP) structures. These systems crystallize into three structures: face centered cubic C15 ( $\text{MgCu}_2$ ), hexagonal C14 ( $\text{MgZn}_2$ ), and double-hexagonal C36 ( $\text{MgNi}_2$ ) [4]. Because of their FCC-based structure, the C15 Laves phases are predicted to exhibit better deformability than the other two Laves phases among the three Laves phase structures [5]. Few studies have been theoretically and experimentally investigated on  $\text{LaCo}_2$  compound. Robertson *et al.* [6] stated that the  $\text{LaCo}_2$  has the cubic  $\text{MgCu}_2$ -type structure with a lattice parameter of 7.449 Å. Another experimental study by Nakamura *et al.* [7] reported on synthesizing

the cubic  $\text{LaCo}_2$  by <sup>59</sup>Co NMR experiments; they concluded the presence weak ferromagnetism in  $\text{LaCo}_2$ . In another work, Sasaki and coworkers [8], studied the magnetic properties of  $\text{LaCo}_2$  in a  $\text{MgCu}_2$  structure by first-principles electronic structure calculations by utilizing the Korringa-Kohn-Rostoker (KKR) method for the electronic structure calculation.

To the best of our knowledge, there is no theoretical work available in the literature on the detailed physical properties of the Lave phase  $\text{LaCo}_2$  compound, which is the central focus of our paper. In this study, we have investigated the structural, elastic and electronic properties of the  $\text{LaCo}_2$  intermetallic compounds in cubic C15 ( $\text{MgCu}_2$ ) phase using first principle calculations, which are followed by the transport properties using semi-classical Boltzmann theory in order to deeply understand the ground-state properties and provide accurate theoretical results.

## 2. Method of calculations

The computation has been performed by using full potential linearized augmented plane wave (FP-LAPW) method within the spin polarized density functional theory (DFT) [9,10] implemented in Wien2k code [11,12]. We have used the generalized gradient approximation GGA with Hubbard (U) as exchange correlation functional [13,14]. The cut-off parameter value used is  $\text{RMT} \cdot K_{\text{max}} = 8$ , (where RMT is the smallest radius in the muffin spheres and  $K_{\text{max}}$  represents the cutoff in the plane wave). The radii of the muffin-tin sphere RMT were 2.5 Bohr for La and 2.41 Bohr for cobalt. The cut-off

energy, which defines the separation among the core and the valence states, was set at  $-7.0$  Ry. The maximum value for partial waves inside the atomic sphere is  $l_{\max} = 10$  while the  $G_{\max}$  parameter was taken to be 12.0. For the Brillouin zone (BZ) integration a tetrahedron method with  $8 \times 8 \times 8$  special k-points in the irreducible wedge of BZ was used [15]. To achieve a correct convergence of all the calculations for our compounds; the Hubbard parameter was employed for the strongly correlated elements. We applied  $U$  on the 3d orbital of Co atoms. Hence, we used the values of Coulomb interaction parameter  $U = 4$  eV and the Exchange parameter  $J = 0.9$  eV [16]. The calculations of the transport properties of  $\text{LaCo}_2$  in C15-Laves phase were performed based on the calculated spin-polarized electronic band structures using the semi-classical Boltzmann theory [17] as implemented in the BoltzTraP code with a dense mesh of 100000 k-points.

### 3. Results and discussions

#### 3.1. Structural properties and formation energy

The Laves phase  $\text{LaCo}_2$  compound investigated in the present work crystallizes in the face centered cubic  $\text{MgCu}_2$  type structure with space group Fd-3m (No. 227). The La atoms occupy the tetrahedral 8a Wyckoff site (1/8, 1/8, 1/8) and the Co atoms occupy the octahedral 16d site (1/2, 1/2, 1/2) [18], as shown in Fig. 1. We used the experimental lattice constant

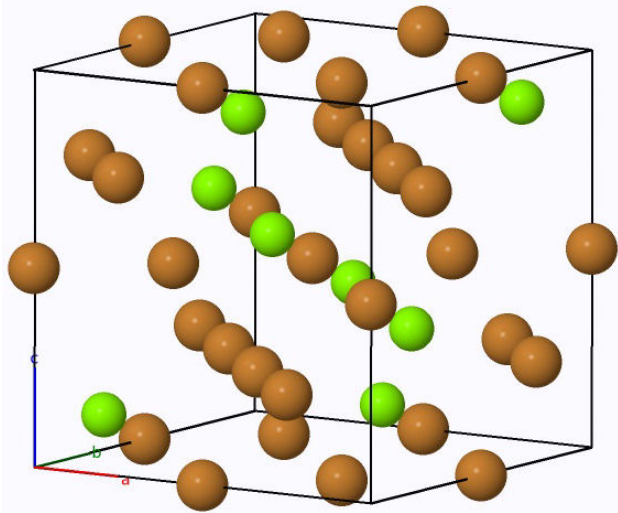


FIGURE 1. Crystal structure of Laves Structure (C15)  $\text{LaCo}_2$ .

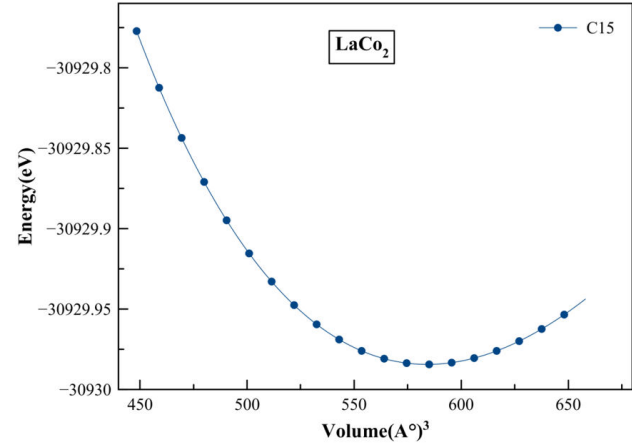


FIGURE 2. Total energy computed against volume for  $\text{LaCo}_2$  in the C15 structure.

to start the calculations. The optimized lattice parameters  $a$ , cell volume  $V$ , bulk modulus  $B$ , and the first pressure derivative of the bulk modulus  $B'$  recorded in Table I, are determined by fitting the total energy per cell with the Birch-Murnaghan equation of state [19,20]. The Energy-optimization curve of  $\text{LaCo}_2$  using GGA approximation is also shown in Fig. 2. The calculated lattice constant of  $\text{LaCo}_2$  intermetallic is  $7.274 \text{ \AA}$  so we can deduce that the experimental and theoretical values are in good agreement.

We therefore measured the formation energy for  $\text{LaCo}_2$  intermetallic compound in order to study the relative phase stability. The formation energy ( $\Delta E$ ) can be calculated by the following expression [21]:

$$\Delta E = E_{\text{LaCo}_2} - (E_{\text{La}}^{\text{DHCP}} + 2E_{\text{Co}}^{\text{HCP}}),$$

where  $E_{\text{La}}^{\text{DHCP}}$  and  $E_{\text{Co}}^{\text{HCP}}$  are the total energies of the elements La and Co atom in their stable bulk structures, and  $E_{\text{LaCo}_2}$  is the equilibrium total energy of the  $\text{LaCo}_2$  compound. The estimated formation energy of  $\text{LaCo}_2$  is included in Table I, it gives the value of  $-0.6211$  (meV) which is negative indicating that this phase is stable from an energy point of view.

#### 3.2. Mechanical stability and elastic properties

The mechanical stability of materials under the effect of hydrostatic pressure has a great influence on their performance in industrial and technological applications. Furthermore elastic stiffness constants of solids are very important

TABLE I. The calculated equilibrium Lattice constant  $a$  ( $\text{\AA}$ ), equilibrium volume  $V$  ( $\text{\AA}^3$ ), bulk modulus  $B$  (GPa), first order pressure derivative  $B'$ , and the formation energy  $\Delta E$  (meV) of the  $\text{LaCo}_2$  compound.

Compound	a			V	B (GPa)	B'	$\Delta E$ (meV)
	Present work	Expt. [6]	Other calculation [8]				
$\text{LaCo}_2$	7.274	7.449	7.13	649.229	4.128	116.239	-0.6211

TABLE II. Calculated elastic constants  $C_{ij}$  (GPa) of  $\text{LaCo}_2$  under hydrostatic pressure up to 90 GPa.

P(GPa)	$C_{11}$	$C_{12}$	$C_{44}$
0	143.41	80.78	21.38
10	174.827	104.081	36.11
20	233.585	142.641	81.516
30	295.221	183.692	109.496
40	305.385	222.054	135.88
50	372.770	240.778	167.335
60	419.55	267.31	180.076
70	471.256	292.356	197.155
80	518.356	318.265	224.561
90	557.53	337.995	245.07

material parameters because they provide a connection between mechanical properties and dynamic information on the nature of the forces operating in solids, in particular for the stability, stiffness, brittleness, ductility, material anisotropy and the propagation of elastic waves in the normal material mode [22].

It is also essential to perform the calculations of the pressure dependence of the elastic constants for  $\text{LaCo}_2$ . Since the intermetallic compound corresponds to the cubic crystal, it has three independent elastic constants  $C_{11}$ ,  $C_{12}$  and  $C_{44}$ . Table II displays the determined elastic constants of  $\text{LaCo}_2$  at pressures of up to 90 GPa. We believe that this is the first work that shows the elastic constants of  $\text{LaCo}_2$  under pressure, and there are no comparable studies in the literature. So our study should encourage the experimental confirmation of these results in future.

From Table II, the measured values of the elastic constants under ambient conditions properly follow the cubic stability criteria [23]:  $C_{11} > 0$ ,  $C_{44} > 0$ ,  $(C_{11} - C_{12}) > 0$ ,  $(C_{11} + 2C_{12}) > 0$ ,  $C_{12} < B < C_{11}$ . Our  $\text{LaCo}_2$  compound in the C15 structure is therefore mechanically stable. But these stability criteria are only valid in the case of zero pressure [24]. For a cubic material under hydrostatic pressure, the generalized stability criteria are summarized as follows:

$$M_1 = \frac{1}{3}(C_{11} + 2C_{12} + P) > 0 \quad (1)$$

$$M_2 = \frac{1}{2}(C_{11} - C_{12} - 2P) > 0 \quad (2)$$

$$M_3 = C_{44} - P > 0. \quad (3)$$

Figure 3 represents the variation of the generalized stability criteria  $M_i$ , as a function of the hydrostatic pressure in an interval of 0 to 90 GPa. According to our calculations, the  $M_i$  values obtained increase with increasing pressure, which means that the  $\text{LaCo}_2$  compound keeps its rigidity under this pressure interval.

An estimation of ductility and brittleness can be provided from the Cauchy pressure value ( $C_{12} - C_{44}$ ), if it is negative the material is expected to be brittle and positive values

as ductile. Furthermore the Cauchy pressure is used to define the angular character of atomic bonding in metals and compounds [25]; a negative value means that the material is nonmetallic with directional bonding and the material is supposed to be metallic if the Cauchy pressure is positive [26]. From Table III, it is evident that the values of the Cauchy pressures of  $\text{LaCo}_2$  at ambient condition and under all the applied pressures are positive approving the ductility and the metallic behavior of this compound.

The Pugh's ratio ( $B/G$ ) [27,28] is an another stability criterion to determinate whether the material is ductile or brittle. If  $B/G > 1.75$  the material is ductile or otherwise brittle. It is evident from Table III that  $\text{LaCo}_2$  compound is ductile at ambient pressure and that the ductility decreases gradually with increasing pressure. This agrees well with the Cauchy pressure estimation.

The polycrystalline elastic moduli can be computed using the Voigt-Reuss-Hill (VRH) method [29], based on the elastic constants. The appropriate equations are given as follows for the cubic structure:

$$G_V = \frac{C_{11} - C_{12} - 3C_{44}}{5}, \quad (4)$$

$$G_R = \frac{5C_{44}(C_{11} - C_{12})}{(4C_{44} + 3[C_{11} - C_{12}])}, \quad (5)$$

$$B_V = B_R = \frac{(C_{11} + 2C_{12})}{5}, \quad (6)$$

$$B = \frac{1}{2}(B_R + B_V), \quad (7)$$

$$G = \frac{1}{2}(G_V + G_R), \quad (8)$$

$$E = \frac{9BG}{3B + G}, \quad (9)$$

$$v = \frac{3B - 2G}{2(3B + G)}. \quad (10)$$

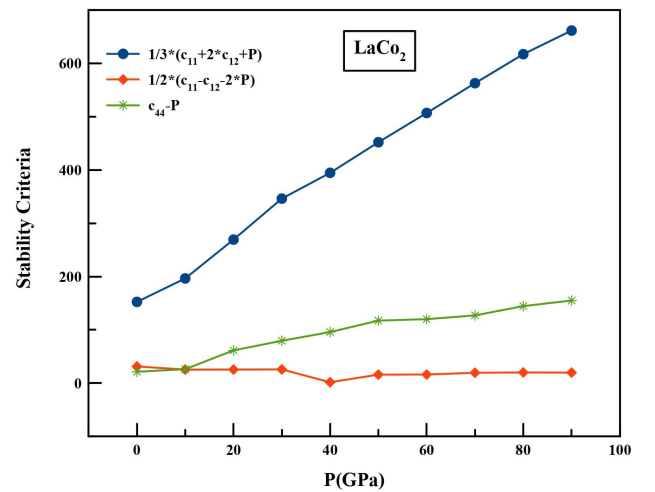

 FIGURE 3. The generalized stability criteria  $M_i$  of the  $\text{LaCo}_2$  compound as a function of pressure.

TABLE III. The calculated bulk modulus  $B$  (GPa), shear modulus  $G$  (GPa), Young's modulus  $E$  (GPa),  $B/G$  values, Poisson's ratio  $\nu$  and anisotropy factor  $A$  of  $\text{LaCo}_2$  compound under hydrostatic pressure.

P(GPa)	$B$	$G$	$E$	$B/G$	$\nu$	$A$	$C_{12} - C_{44}$
0	101.657	24.921	70.224	4.079	0.385	0.683	59.4
10	127.663	35.813	98.257	3.565	0.372	1.021	67.971
20	172.955	64.495	178.245	2.682	0.348	1.793	61.125
30	220.868	83.519	233.057	2.645	0.344	1.964	74.196
40	249.831	84.786	260.459	2.947	0.346	3.261	86.174
50	284.775	115.232	331.237	2.471	0.328	2.536	73.442
60	318.057	127.476	362.819	2.495	0.331	2.366	87.234
70	351.99	143.569	403.365	2.452	0.330	2.204	95.202
80	384.962	163.339	455.361	2.371	0.324	2.245	93.704
90	411.173	177.544	496.057	2.316	0.320	2.233	92.925

Here,  $B$ ,  $G$  and  $E$  are the polycrystalline bulk modulus, shear modulus and Young's modulus, respectively.  $\nu$  is the Poisson ratio.

Figure 4 shows the pressure dependence of bulk, shear, and Young's moduli of C15-type  $\text{LaCo}_2$ . It is clearly seen that the value of  $B$ , which represents the resistance of the crystal to the volumetric change, increases with the increase of the pressure, which means that the presence of external pressure increases resistance to deformation.

Additionally, the shear moduli and Young's modulus are the measure of resistance to reversible deformation by the applied shear force. The value of  $G$  and  $E$  increases with increasing the external pressure. this implies that, for  $\text{LaCo}_2$  the resistance to shear deformation and the stiffness are increased with the increase of pressure respectively.

Poisson's ratio  $\nu$  is another rule used for determining the ductility and brittleness of a compound. The material has a ductile nature if its value is greater than 0.26; otherwise, the material is considered to be brittle. Table III shows that Pois-

son's ratio for  $\text{LaCo}_2$  is greater than 0.26, which confirms its ductile nature. Poisson's ratio  $\nu$  also gives knowledge about the bonding nature in a material. According to this limit the type of material bonding will be ionic if  $\approx 0 : 25$ , covalent if  $\approx 0 : 10$  and metallic if  $\approx 0 : 33$ . For our compounds the  $\nu$  is found close to 0.33 and hence major bonding in these materials is metallic [30].

Zener's anisotropy factor ( $A$ ) reveals the degree of the elastic anisotropy of the solid. For a perfectly isotropic material,  $A$  will take the value equal to 1; deviation from 1 shows anisotropic nature of the material [31,32]. For  $\text{LaCo}_2$  the values of  $A$  which are listed in Table III, are calculated by using the following formula at different pressures:

$$A = \frac{C_{44}}{C_{11} - C_{12}} \quad (11)$$

The determined values of  $A$  are found to be different than unity, suggesting the material will have elastic anisotropic nature.

In addition, the melting temperature, which is another thermodynamic quantity, has been determined using the following empiric expression as mentioned below [33,34].

$$T_m(\text{K}) = [553(\text{K}) + (5.911)C_{11}] \text{ GPa} \pm 300 \text{ K} \quad (12)$$

The corresponding value observed for the present alloy is  $1400.69 \pm 300 \text{ K}$  thus shows that the material has a great capacity to preserve its crystal structure over a wide range of temperatures.

### 3.3. Electronic properties

Figure 5 displays the computed spin-polarized band structures for  $\text{LaCo}_2$  at the measured equilibrium lattice constants along with the high symmetry directions in the Brillouin zone using the GGA+U method. This figure shows, in both spin configurations, an overlap between the valence and the conduction bands around the Fermi level. In addition, at the Fermi level there is no band gap, which indicates the metallic nature of our compound.

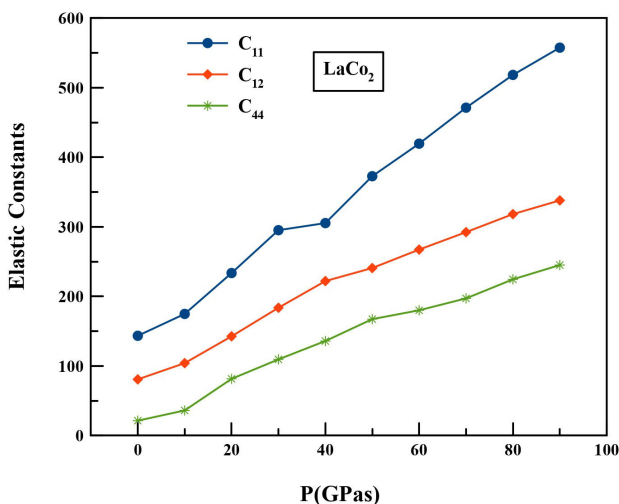


FIGURE 4. The pressure dependence of bulk, shear, and Young's moduli of C15-type  $\text{LaCo}_2$ .

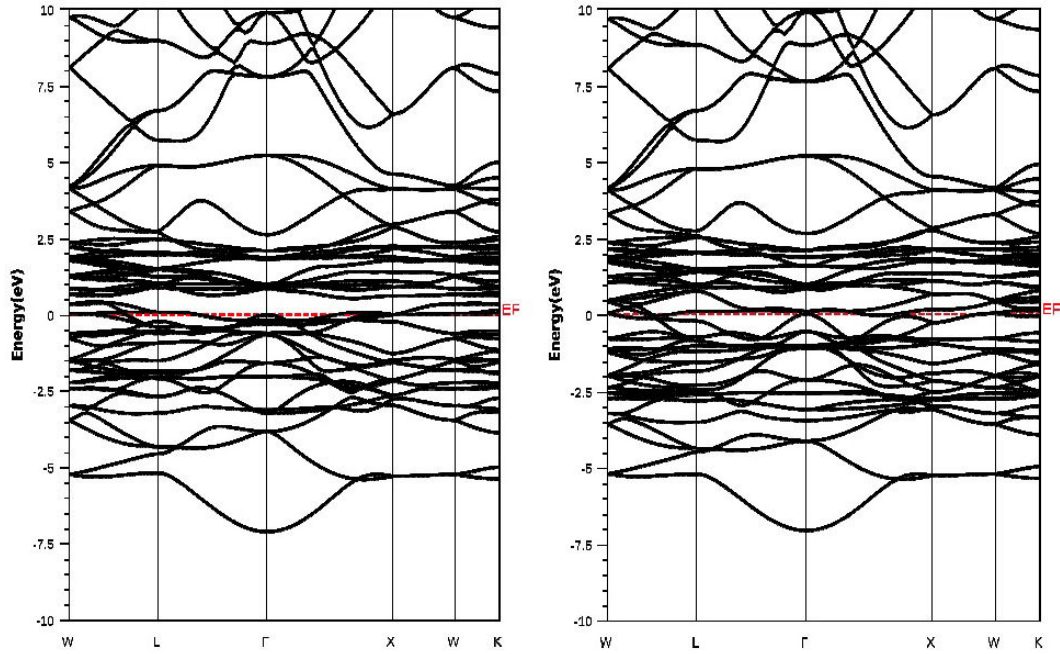


FIGURE 5. Band structures of  $\text{LaCo}_2$  obtained within GGA + U for spin down and spin up configurations.

It is well known that the density of states at  $E_F$ ,  $N(E_F)$  tends to uncommon transport properties, since both spin-up and spin-down densities contribute to the  $E_F$  states. Analogous behavior has been reported in  $\text{TbFe}_2$ ,  $\text{TbCo}_2$  and  $\text{RENi}_2$  ( $\text{RE} = \text{Dy, Ho}$  and  $E_r$ ) compounds [35,36]. Consequently, the bands which cross  $E_F$  are responsible for the transport properties of the compound and the bands which do not cross  $E_F$  can make a negligible contribution to the transport properties [35].

Furthermore, the total density of states of the compound (for all atoms in a unit cell) and the partial DOS (per atom) were determined using GGA + U approximation. The curve is shown in Fig. 6. The spin-up and spin-down, along with the TDOS, are found to be anti-symmetrical, which indicates that the  $\text{LaCo}_2$  is in a ferromagnetic state. These findings can be due to the contribution of the 3d states of cobalt (Co) and the contribution of the 4f states of Lanthane (La) as well to the TDOS.

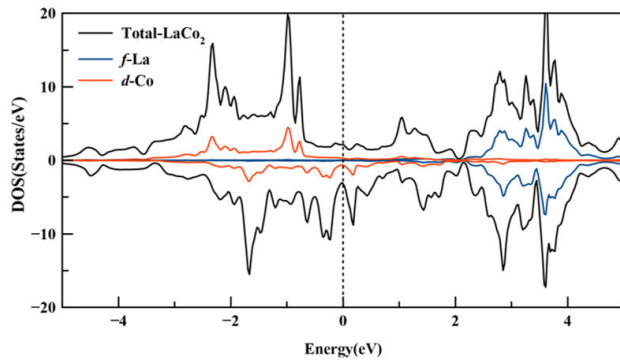


FIGURE 6. The total and partial density of states of  $\text{LaCo}_2$  (spin up and spin down) obtained with GGA + U calculations.

Moreover, the energy dispersion spectrum is observed to cross the Fermi level ( $E_F = 0$  eV), which is another indicator that this compound is potentially electrically conductor. Indeed, the low energy region, which is located around  $-5$  and  $0$  eV, is mainly filled by the d states of the Co atoms. The region above ( $E_F = 0$ ) from  $2$  to  $4$  eV is dominated by 4f states of Lanthane (La) and the majority of the total DOS (from  $-5$  to  $+2$  eV) is governed by the 3d states of Co.

### 3.4. Transport properties

The thermoelectric properties were performed within relaxation time approximation implemented in the BoltzTrap code, based on the Boltzmann transport theory. Effective thermoelectric materials should have high electrical conductivity ( $\sigma/\tau$ ), large Seebeck coefficient ( $S$ ) and low thermal conductivity ( $k_e/\tau$ ). We need to maintain the density and mobility of the charge carriers in order to achieve maximum electrical conductivity.

#### 3.4.1. Electrical conductivity

To ensure that the examined compound is sufficient to provide maximum effectiveness in the  $E$  region. We have plotted the electrical conductivity of  $\text{LaCo}_2$  compound at three constant temperatures  $300$ ,  $600$  and  $900$  K as a function of chemical potential ( $\mu - E_F = \pm 2$  eV) for both spin polarized channels as shown in Fig. 7. From the figure, we can see that for spin up channel of  $\text{LaCo}_2$  a remarkable rise in electrical conductivity occurs just above and below  $E_F$  to attain the maximum value of approximately  $3.73 \times 10^{20} (\Omega\text{ms})^{-1}$  around  $\mu - E_F = -0.11$  eV at temperature  $300$  K for  $n$ -type conduction, and  $3.78 \times 10^{20} (\Omega\text{ms})^{-1}$  at  $300$  K around

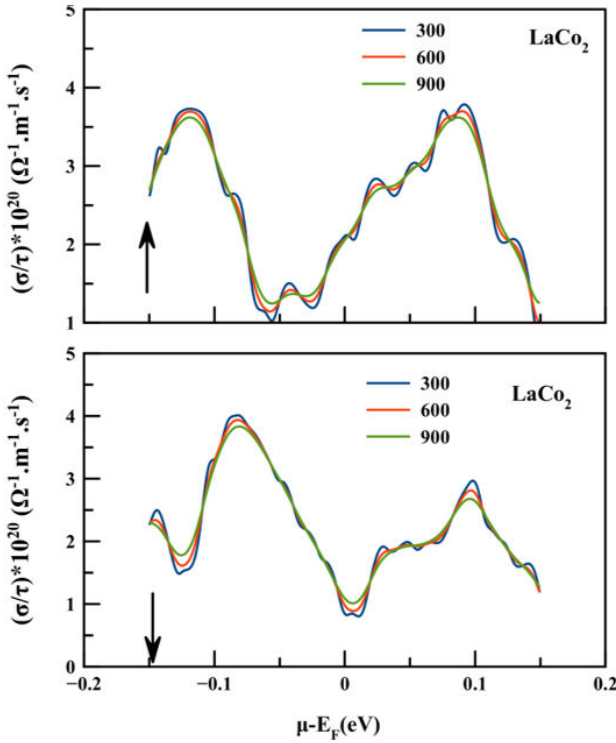


FIGURE 7. The electrical conductivity of  $\text{LaCo}_2$  for both spin configurations as a function of chemical potential at three constant temperatures (300, 600 and 900) K.

$\mu - E_F = 0.09$  eV for  $p$ -type conduction. While for the spin down case a maximum value of about  $4.01 \times 10^{20} (\Omega\text{ms})^{-1}$  was achieved at 300 K and  $\mu - E_F = -0.08$  eV for  $n$ -type conduction and about  $2.96 \times 10^{20} (\Omega\text{ms})^{-1}$  at 300 K and  $\mu - E_F = -0.09$  eV for  $p$ -type conduction.

It is obvious from the above interpretation that the holes play a major role in achieving the highest values of electrical conductivity in the spin up configuration and that the electrons play an important role in the spin-down configuration.

### 3.4.2. Electronic thermal conductivity

The thermal conductivity is generally composed of two parts, the first one coming from the electronic contribution  $\kappa_e$  (electron or hole) and the second one generated by lattice thermal conductivity  $\kappa_l$  (phonon contribution). We should underline that BoltzTraP code only calculates the electronic part  $\kappa_e$ .

The electronic thermal conductivity is measured as a function of chemical potential ( $\mu - E_F = \pm 0.15$  eV) for both spin configurations of  $\text{LaCo}_2$  compound. Figure 8 shows that a significant increase in thermal conductivity occurs with an increase in temperature. And the temperature 900 K generated the highest  $\kappa\tau$  values, while 300 K is the adequate temperature giving the lowest  $\kappa\tau/e$  values within the chemical potential range  $\mu - E_F = +0.15$  eV. So the materials studied provided optimal efficiency in this range of chemical potential.

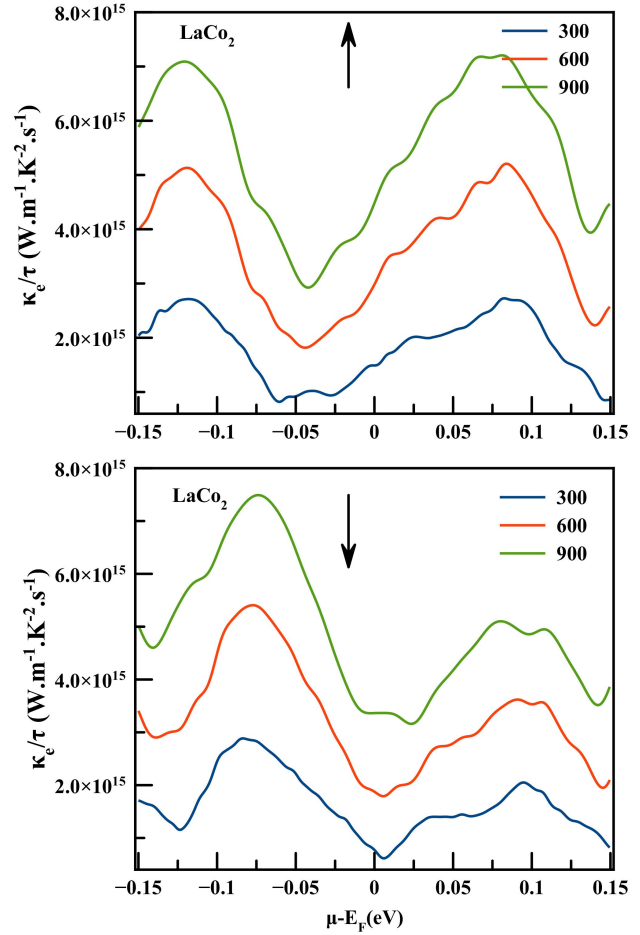


FIGURE 8. The electronic thermal conductivity of  $\text{LaCo}_2$  for both spin configurations as a function of chemical potential at three constant temperatures (300, 600 and 900) K.

### 3.4.3. Seebeck coefficient (Thermopower)

The Seebeck coefficient indicates the magnitude of an induced thermoelectric voltage regarding the temperature difference throughout the material [1]. Positive Seebeck coefficient values signify that hole-type carriers dominate the thermoelectric transport in the material, while negative values of the Seebeck coefficient signify the dominance of electron type carriers.

Figure 9 illustrates the chemical potential ( $\mu - E_F = \pm 0.2F$  eV) dependence of Seebeck coefficient of  $\text{LaCo}_2$  compound at temperature values of 300 K, 600 K and 900 K for both spin configurations. It has been found that for spin up channel of  $\text{LaCo}_2$  the highest value of Seebeck coefficient for  $p$ -type conduction of about  $64.02 \mu\text{V/K}$  is achieved at 300 K for  $\mu - E_F = 0.14$  eV. And for  $n$ -type conduction of about  $-29.83 \mu\text{V/K}$  at 900 K for  $\mu - E_F = -0.014$  eV. While for spin down channels the highest value of Seebeck coefficient for  $p$ -type conduction is about  $45.74 \mu\text{V/K}$  at 300 K for  $\mu - E_F = 0.14$  eV, while for  $n$ -type conduction is about  $-47.09 \mu\text{V/K}$  at 600 K for  $\mu - E_F = 0.017$  eV.

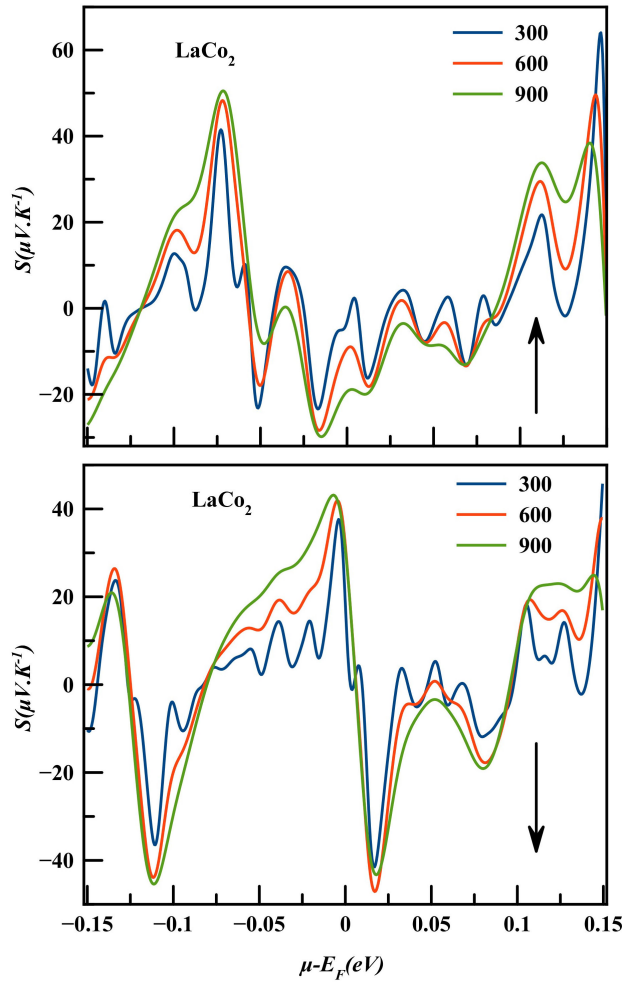


FIGURE 9. The Seebeck coefficient of  $\text{LaCo}_2$  for both spins configurations as a function of chemical potential at three constant temperatures (300, 600 and 900) K.

#### 3.4.4. Power factor ( $P$ )

The power factor ( $\text{PF} = S^2\sigma$ ), which is essential to explore the efficiency of the thermoelectric material, is plotted against chemical potential  $\mu - E_F = \pm E$  0.15 eV in Fig. 10 at three temperatures 300, 600 and 900 K for both spin configurations of  $\text{LaCo}_2$ . In the spin up channel, the highest value of power factor of about  $4.1 \times 10^{14}$   $\text{W/mK}^2\text{s}$  is achieved at 900 K for  $\mu - E_F = -0.07$  eV,  $2.42 \times 10^{14}$   $\text{W/mK}^2\text{s}$  is achieved at 600 K for  $\mu - E_F = -0.07$  eV and  $1.16 \times 10^{14}$   $\text{W/mK}^2\text{s}$  is achieved at 300 K for  $\mu - E_F = 0.14$  eV. Although the spin down channel, shows the highest value of about  $4.5 \times 10^{14}$   $\text{W/mK}^2\text{s}$  at 900 K for  $\mu - E_F = -0.1$  eV and  $2.67 \times 10^{14}$   $\text{W/mK}^2\text{s}$  at 600 K for  $\mu - E_F = -0.11$  eV, while it is  $0.92 \times 10^{14}$   $\text{W/mK}^2\text{s}$  at 300 K for  $\mu - E_F = -0.11$  eV.

## 4. Conclusion

Overall, we have investigated the structural, elastic, electronic, and thermoelectric properties of Laves phase  $\text{LaCo}_2$

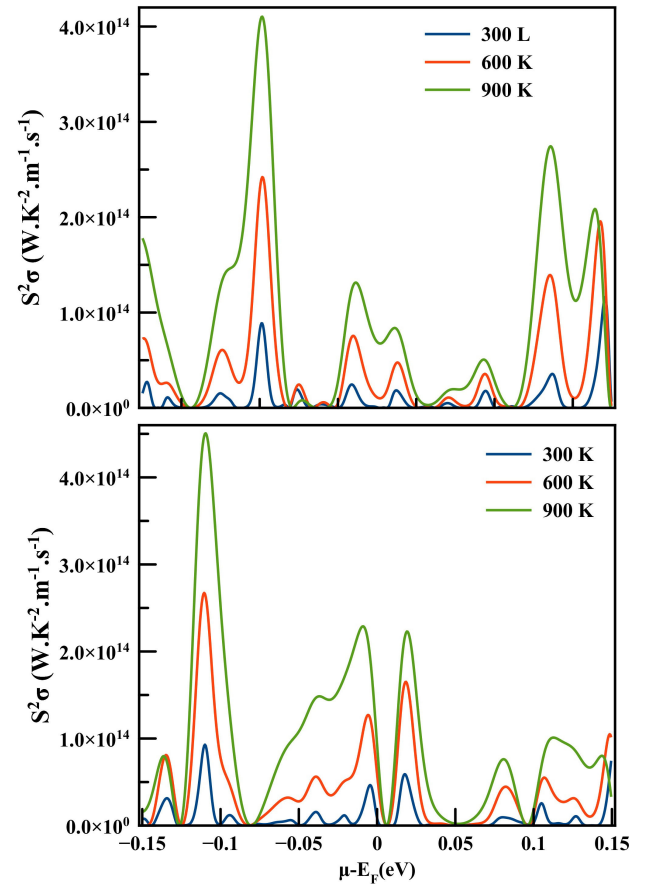


FIGURE 10. The power factor of  $\text{LaCo}_2$  for both spin configurations as a function of chemical potential at three constant temperatures (300, 600 and 900) K.

using FP-LAPW method with GGA+U approximation for exchange and correlation effect and using the Boltzmann transport equation. The equilibrium lattice parameters evaluated are consistent with other data values cited in the previous studies. We have measured and discussed for the first time the elastic constants, Cauchy pressure, bulk modulus, shear modulus, Young's modulus, of the cubic laves phase intermetallic compound  $\text{LaCo}_2$ . The research suggests that according to the elastic stability of the C15 structure,  $\text{LaCo}_2$  is mechanically stable with a pressure range of 0 to 90 GPa. The investigated Cauchy pressure, Pugh's ratio and Poisson's ratio of this Laves phase indicate the ductile nature. From the band structure diagram, the valance and conduction bands are overlapped with each other at Fermi level, indicating that the material possesses metallic characteristics. In addition, transport coefficients including electrical conductivity, thermal conductivity, Seebeck coefficient and power factor have been determined using BoltzTraP code. The increase in the Seebeck coefficient leads directly to the rise of the power factor which is extremely high, making our compound an ideal candidate for spin-voltage generator components.

1. D. J. Thoma, Intermetallics: Laves Phases. Encyclopedia of Materials: Science and Technology, edited by K. H. Jürgen Buschow *et al.*, 2nd ed. (Pergamon, Oxford, 2001), 10.1016/b0-08-043152-6/00739-7
2. M. U. Salma, M. A. Rahman, M. I. Kholil, and M. S. Ali, (2019) MgCu<sub>2</sub>-type laves phases CaPt<sub>2</sub>, SrPd<sub>2</sub> and SrPt<sub>2</sub>: A DFT based ab-initio investigation. *Solid State Commun.* **296** (2019) 1,10.1016/j.ssc.2019.03.012
3. E. Gratz, and A. S. Markosyan, Physical properties of RCo<sub>2</sub>Laves phases. *Journal of Physics: Condensed Matter*, **13** (2001) (23)R385. doi:10.1088/0953-8984/13/23/202
4. M. I. Kholil, M. Z. Rahaman, and M. A. Rahman, First principles study of the structural, elastic, electronic, optical and thermodynamic properties of SrRh 2 laves phase intermetallic compound. *Comput. Condens. Matter* **13** (2017) 65. url10.1016/j.cocom.2017.09.008
5. X. Zhang *et al.*, Structural, elastic, and thermal properties of Laves phase ZrV<sub>2</sub> under pressure. *J. Appl. Phys.* **109** (2011) 113523, <https://doi.org/10.1063/1.3590707>.
6. D. L. Robertson, J. F. Cannon, and H. T. Hall, High-pressure and high-temperature synthesis of LaCo<sub>2</sub>. *Mater. Res. Bull.*, **7** (1972) 977, [https://doi.org/10.1016/0025-5408\(72\)90088-8](https://doi.org/10.1016/0025-5408(72)90088-8).
7. H. Nakamura *et al.*, Evidence of Spontaneous Co Moment in a Rare-Earth-Cobalt Laves Phase Compound.<sup>59</sup>Co NMR Study of LaCo<sub>2</sub>. *J. Phys. Soc. Jpn.*, **71** (2002) 2117. <https://doi.org/10.1143/JPSJ.71.2117>.
8. S. Sasaki *et al.*, First-principles Electronic Structure Calculation of LaCo<sub>2</sub> in MgCu<sub>2</sub> Structure, *J. Phys. Soc. Jpn.* **76** (2007) 084711, <https://doi.org/10.1143/JPSJ.76.084711>.
9. P. Hohenberg and W. Kohn, Inhomogeneous Electron Gas, *Phys. Rev.* **136** (1964) B864. <https://doi.org/10.1103/PhysRev.136.B864>.
10. W. Kohn, and L. J. Sham, Self-Consistent Equations Including Exchange and Correlation Effects. *Effects, Phys. Rev.*, **140** (1965) A1133. <https://doi.org/10.1103/PhysRev.140.A1133>.
11. P. Blaha *et al.*, *An Augmented Plane Wave Plus Local Orbitals Program for Calculating Crystal Properties*, Vienna University of Technology, Vienna, Austria, 2001.
12. M. Berber *et al.*, Structural, electronic, and optical properties of quaternary alloys Al<sub>0.50</sub>Ga<sub>0.50</sub>NxSb<sub>1-x</sub>: a first principles study. *Rev. Mex. Fis.* **66** (2020) 790. <https://doi.org/10.31349/RevMexFis.66.790>
13. J. P. Perdew and A. Zunger, Self-interaction correction to density-functional approximations for many-electron systems, *Phys. Rev. B* **23** (1981) 5048, <https://doi.org/10.1103/PhysRevB.23.5048>.
14. V. I. Anisimov *et al.*, Density-functional theory and NiO photoemission spectra. *Phys. Rev. B*, **48** (1993) 16929. doi:<https://doi.org/10.1103/PhysRevB.48.16929>.
15. H. J. Monkhorst, and J. D. Pack, Special points for Brillouin-zone integrations. *Phys. Rev. B*, **13** (1976) 5188. <https://doi.org/10.1103/PhysRevB.13.5188>.
16. V. I. Anisimov, J. Zaanen, and O. K. Andersen, Band theory and Mott insulators: Hubbard *U* instead of Stoner *I*. *Phys. Rev. B* **44** (1991) 943. <https://doi.org/10.1103/PhysRevB.44.943>.
17. G. K. H. Madsen, and D. J. Singh, BoltzTra P. A code for calculating band-structure dependent quantities. *Comput. Phys. Commun.*, **175** (2006) 67. <https://doi.org/10.1016/j.cpc.2006.03.007>.
18. A. Bentouaf, R. Mebsout, H. Rached, S. Amari, A. H. Re-shak, and B. Aïssa, Theoretical investigation of the structural, electronic, magnetic and elastic properties of binary cubic C15-Laves phases TbX<sub>2</sub> (X = Co and Fe) *J. Alloys Compd.* **689** (2016) 885. <https://doi.org/10.1016/j.jallcom.2016.08.046>.
19. F. D. Murnaghan, The Compressibility of Media under Extreme Pressures. *Proc. Natl. Acad. Sci. U.S.A.* **30** (1944) 244, <https://doi.org/10.1073/pnas.30.9.244>.
20. L. F. Blaha, A. Maafa, A. Chahed, M.A.H. Boukli, A. Sayade, The first principle calculations of structural, magneto-electronic, elastic, mechanical, and thermoelectric properties of half-metallic double perovskite oxide Sr<sub>2</sub>TiCoO<sub>6</sub>. *Rev. Mex. Fis.* **67** (2021) 114. <https://doi.org/10.31349/RevMexFis.67.114>
21. A. A. Mousa, B. A. Hamad, and J. M. Khalifeh, Structure, electronic and elastic properties of the NbRu shape memory alloys. *Eur. Phys. J. B*, **72** (2009) 575, <https://doi.org/10.1140/epjb/e2009-00375-0>.
22. J.-Y. Wang and Y.-C. Zhou, Polymorphism of Ti<sub>3</sub>SiC<sub>2</sub> ceramic: First-principles investigations. *Phys. Rev. B*, **69** (2004) 144108, <https://doi.org/10.1103/PhysRevB.69.144108>.
23. O. Benguerine *et al.*, Structural, elastic, electronic and magnetic properties of Ni<sub>2</sub>MnSb, Ni<sub>2</sub>MnSn and Ni<sub>2</sub>MnSb<sub>0.5</sub>Sn<sub>0.5</sub> magnetic shape memory alloys, *Rev. Mex. Fis.* **66** (2020) 121, <https://doi.org/10.31349/RevMexFis.66.121>.
24. R. O. Jones, and O. Gunnarsson, The density functional formalism, its applications and prospects. *Rev. Mod. Phys.* **61** (1989) 689, <https://doi.org/10.1103/RevModPhys.61.689>.
25. S. A. Dar, R. Sharma, V. Srivastava, and U. K. Sakalle, Investigation on the electronic structure, optical, elastic, mechanical, thermodynamic and thermoelectric properties of wide band gap semiconductor double perovskite Ba<sub>2</sub>InTaO<sub>6</sub>, *RSC Adv.* **9** (2019) 9522, <https://doi.org/10.1039/C9RA00313D>.
26. Y. Liu *et al.*, First-principles investigation of structural and electronic properties of MgCu<sub>2</sub> Laves phase under pressure. *Intermetallics*, **31** (2012) 257. <https://doi.org/10.1016/j.intermet.2012.07.017>.
27. S. F. Pugh, XCII. Relations between the elastic moduli and the plastic properties of polycrystalline pure metals. London Edinburgh Dublin Philos. Mag. J. Sci. **45** (2009) 823, <https://doi.org/10.1080/14786440808520496>.

28. S. Tab, A. Boudali, M. Berber, M. Driss khodja, O. Lhaj El Hachemi, H. Moujr, Structural, elastic, electronic, and magnetic properties of quaternary alloys  $\text{BBi}_{0.75}\text{Mn}_{0.125}\text{N}_{0.125}$ : a first-principles study. *Rev. Mex. Fis* **66** (2020) 627, <https://doi.org/10.31349/RevMexFis.66.627>
29. R. Hill, The Elastic Behaviour of a Crystalline Aggregate. *Proc. Phys. Soc. A*, **65** (1952) 349. <https://doi.org/10.1088/0370-1298/65/5/307>.
30. S. A. Dar, M. A. Ali, and V. Srivastava, Investigation on bismuth-based oxide perovskites  $\text{MBiO}_3$  (M=Rb, Cs, Tl) for structural, electronic, mechanical and thermal properties. *Eur. Phys. J. B* **93** (2020) 102, <https://doi.org/10.1140/epjb/e2020-10073-x>.
31. S. A. Khandy, and D. C. Gupta, Magneto-electronic, Mechanical, Thermoelectric and Thermodynamic Properties of Ductile Perovskite  $\text{Ba}_2\text{SmNbO}_6$ , *Mater. Chem. Phys.* **239** 121983, <https://doi.org/10.1016/j.matchemphys.2019.121983>.
32. S. A. Dar, V. Srivastava, and U. K. Sakalle, Structural, elastic, mechanical, electronic, magnetic, thermoelectric and thermodynamic investigation of half metallic double perovskite oxide  $\text{Sr}_2\text{MnTaO}_6$ , *J. Magn. Magn. Mater.* **484** (2019) 298, <https://doi.org/10.1016/j.jmmm.2019.04.048>.
33. K. Bencherif *et al.*, First Principles Investigation of the Elastic, Optoelectronic and Thermal Properties of Xrubsb: (X=V, Nb, Ta) Semi-Heusler Compounds Using the mBJ Exchange Potential, *J. Electron. Mater.* **45** (2016) 3479, <https://doi.org/10.1007/s11664-016-4488-3>.
34. S. A. Dar, V. Srivastava, U. K. Sakalle, and S. A. Khandy, Ab Initio Investigation on Electronic, Magnetic, Mechanical, and Thermodynamic Properties of  $\text{AMO}_3$  (A=Eu, M=Ga, In) Perovskites, *J. Supercond. Novel Magn.* **31** (2018) 1549, <https://doi.org/10.1007/s10948-017-4365-1>.
35. A. H. Reshak, Thermoelectric properties of  $\text{TbFe}_2$  and  $\text{TbCo}_2$  in C15- laves phase: Spin-polarized DFT+U approach. *J. Magn. Magn. Mater.* **422** (2017) 287, <https://doi.org/10.1016/j.jmmm.2016.09.037>.
36. H. Pawar, M. Aynyas, and S. P. Sanyal, Thermoelectric properties of rare-earth based  $\text{RENi}_2$  (RE=Dy, Ho and Er) Laves phase compounds. *J. Magn. Magn. Mater.*, **468** (2018) 123. <https://doi.org/10.1016/j.jmmm.2018.07.085>.